Title: Chromosome-specific maturation of the epigenome in the Drosophila male germline

James Anderson[1], Steven Henikoff[1,2]*, Kami Ahmad[1]*

[1]Basic Sciences Division, Fred Hutchinson Cancer Center; Seattle, WA, 98109, USA
[2]Howard Hughes Medical Institute; Chevy Chase, MD, USA

*Co-corresponding authors: steveh@fredhutch.org, kahmad@fredhutch.org

Keywords
Epigenetics, epigenome, male germline, spermatogenesis, sex chromosomes, dosage compensation

Abstract
Spermatogenesis in the Drosophila male germline proceeds through a unique transcriptional program controlled both by germline-specific transcription factors and by testis-specific versions of core transcriptional machinery. This program includes the activation of genes on the heterochromatic *Y* chromosome, and reduced transcription from the *X* chromosome, but how expression from these sex chromosomes is regulated has not been defined. To resolve this, we profiled active chromatin features in the testes from wildtype and meiotic arrest mutants and integrate this with single-cell gene expression data from the Fly Cell Atlas. These data assign the timing of promoter activation for genes with germline-enriched expression throughout spermatogenesis, and general alterations of promoter regulation in germline cells. By profiling both active RNA polymerase II and histone modifications in isolated spermatocytes, we detail widespread patterns associated with regulation of the sex chromosomes. Our results demonstrate that the *X* chromosome is not enriched for silencing histone modifications, implying that sex chromosome inactivation does not occur in the Drosophila male germline. Instead, a lack of dosage compensation in spermatocytes accounts for the reduced expression from this chromosome. Finally, profiling uncovers dramatic ubiquitinylation of histone H2A and lysine-16 acetylation of histone H4 across the *Y* chromosome in spermatocytes that may contribute to the activation of this heterochromatic chromosome.

Introduction

The germline in animals is responsible for producing the specialized gametes that transmit genetic information to the next generation, and gene expression in these cells is tightly controlled to ensure proper cell differentiation and genome stability. In many cases gene regulation is distinctive from that in somatic cells (Freiman, 2009). A dramatic example of this is the deployment of testis-specific variants of core transcriptional machinery in the Drosophila male germline that are used to activate and regulate gene promoters during sperm development (Hiller et al., 2004). These variants enable the activation of testis-specific promoters, but the effects they have on transcription and chromatin are less characterized.

Gene regulation in Drosophila spermatogenesis also involves widespread changes on entire chromosomes. The sex chromosomes each have distinct chromosomal features which uniquely

impact their expression in the germline: the single *X* chromosome of males is thought to be upregulated in early germline cells, but then suffers a broad reduction in expression during spermatogenesis (Witt et al., 2021; Mahadevaraju et al., 2021). In contrast, the *Y* chromosome is largely heterochromatic and silenced in somatic cells but becomes highly active in spermatocytes, extruding long, diffuse loops of actively transcribing genes within the nucleus (Fingerhut et al., 2019). How these chromosome-wide changes are orchestrated remains unknown.

Here, we apply CUT&Tag chromatin profiling (Kaya-Okur et al., 2019) on the adult testis of Drosophila to characterize the chromatin features of the spermatogenic transcription program. By integrating chromatin profiles with published single-cell transcriptional data for the Drosophila testis, we track active chromatin features of germline-specific gene promoters, detailing their timing of activation. Further, we describe the enrichment of RNA polymerase II and select histone modifications across the sex chromosomes in isolated spermatocytes. These profiles show that the *X* chromosome does not accumulate repressive chromatin marks, supporting a model where reduced expression of this chromosome is due to a lack of chromosomal dosage compensation in this cell type. Surprisingly, we find that high levels of mono-ubiquitinylated histone H2A accumulate across the *Y* chromosome in spermatocytes, implicating this otherwise repressive histone modification in the activation of heterochromatic regions in the male germline.

Results

Profiling active promoters in the Drosophila testes

To profile chromatin features of gene activity during spermatogenesis, we performed CUT&Tag profiling for histone H3 lysine-4 dimethylation (H3K4me2), which marks active promoters and enhancers (Bernstein et al., 2005). The adult testis contains all developmental stages of spermatogenesis, as cells in the germline continually proliferate and differentiate (**Figure 1A**) (White-Cooper & Bausek, 2010). Germline stem cells at the apical tip of the testis asymmetrically divide to birth a gonialblast; these undergo four mitotic divisions and then complete one final S phase before entering an extended G2 phase as primary spermatocytes before meiosis and differentiation into sperm. The transcriptional program of premeiotic and post-meiotic stages has been detailed most extensively by single-cell RNA-seq profiling (Witt et al., 2019; Shi et al., 2020; Witt et al., 2021; Mahadevaraju et al., 2021; Raz et al., 2023). To assess the developmental timing of active chromatin features, we profiled the H3K4me2 modification in wildtype adult testes and in two stage-arrest mutants. The germline of *bag-of-marbles* (*bam*) mutant males arrests in the spermatogonial stage, so their testes are full of early germline cells (Chen et al., 2011). The germline of *always early* (*aly*) mutants arrests in the early primary spermatocyte stage, thus enriching for this cell type (Laktionov et al., 2018). Between these three genotypes, only wildtype testes contain late spermatocytes and post-meiotic stages. Thus, profiling testes from these flies distinguishes when in development active chromatin features appear. We dissected testes from one-day-old adult wildtype, *bam*, and *aly* males, sequenced three replicate libraries for each genotype, and mapped reads to a repeat-masked version of the Drosophila dm6 genome assembly (see Methods). To aid distinguishing germline from somatic cell type chromatin features, we also profiled wing imaginal discs from larvae. Sequencing from replicates was pooled, providing 4.4M-19.2M reads/genotype, and publicly available coverage tracks are posted

88 (https://genome.ucsc.edu/s/jamesanderson12358/analysis230508___UCSC_session_germline_MS
89).
90
91 Inspection of these tracks reveals active chromatin features that track with gene expression timing
92 during spermatogenesis. For example, the promoter for the germline stem cell marker *nanos* (*nos*)
93 is marked with the H3K4me2 modification in *bam* testes, with less signal in *aly* or in wildtype testes
94 (**Figure 1B**). In contrast, the promoter of the spermatocyte-expressed gene *loopin-1* lacks the
95 H3K4me2 modification in *bam* testes but is heavily marked in *aly* and in wildtype testes (**Figure**
96 **1C**). Similarly, the promoter of the meiotically-expressed genes *Mst36Fa* and *Mst36Fb* (Di Cara et
97 al., 2006) are marked with the H3K4me2 modification in wildtype testes where the later stages of
98 spermatogenesis are present (**Figure 1D**). In contrast, no signal is present at the *nos*, *loopin-1*,
99 *Mst36Fa* or *Mst36Fb* genes in wing discs (**Figure 1B-D**). Finally, profiles for all three testes
100 samples show the H3K4me2 mark at the promoters of the homeotic genes *abdominal-A* and
101 *Abdominal-B* that are expressed in the somatic cells of the testis (**Figure 1E**), since somatic cells
102 are present in all three samples.

103 To visualize chromatin features across active promoters during spermatogenesis, we categorized
104 genes by their timing and level of mRNA expression in the male germline in single-nucleus RNA-
105 seq profiling (Raz et al., 2023). We focused on five categories of genes with germline-enriched
106 expression in germline stages (**Supplementary Figure 1, Supplementary Table 2, 3**), including
107 845 genes that are predominantly expressed in spermatogonia, 1,510 expressed in early
108 spermatocytes, 1,524 expressed in mid-spermatocytes, 2,052 expressed in late spermatocytes, and
109 475 genes expressed in spermatids. We then displayed the summed H3K4me2 signal spanning -
110 200 – +500 bp around each of the promoters for these genes (**Figure 2A**). In the whole testis,
111 germline stages compose a small proportion of all cells, and so genes specifically expressed in
112 these stages have low signal for both mRNA and the H3K4me2 modification (**Supplementary**
113 **Table 2**). Nevertheless, the overall tendency is that promoters of genes expressed in
114 spermatogonia are marked with the H3K4me2 modification in *bam* mutant testes, which are
115 enriched for early stages compared to *aly* mutant and wildtype testes (**Figure 2A**). For example, the
116 promoters of early germline markers *nos*, *vasa* (*vas*), and *zero population growth* (*zpg*) are each
117 heavily marked with H3K4me2 in *bam* mutant samples, reflecting their activity (**Figure 2A,B**).
118 Similarly, the promoters for many genes primarily expressed in early spermatocytes and mid-stage
119 spermatocytes are often most heavily marked with H3K4me2 in bam mutant testes, implying that
120 these genes first become active in spermatogonia and accumulate mRNA in spermatocyte stages.
121 Finally, gene promoters for mRNA that accumulate in late spermatocytes and in differentiating
122 spermatids are predominantly marked with the H3K4me2 modification in wildtype testes, as this is
123 the only sample that contains these stages of spermatogenesis (**Figure 2A**). This includes the
124 activation of promoters for the *Y* chromosome-linked fertility factor genes (*kl-2*, *kl-3*, and *kl-5*) which
125 are primarily expressed in late spermatocytes (**Figure 2A,B**). However, the activation timing of
126 these genes appear to differ, as the promoters of *kl-2* and *kl-3* accumulate the H3K4me2
127 modification earlier than does the *kl-5* promoter (**Figure 2B**). The most dramatic instance of
128 precocious activation of a *Y*-linked promoter is the *FDY* gene which becomes active in early
129 spermatocytes, matching its early production of mRNA (**Figure 2A,B**).

130 There are three exceptions to the overall trend of correspondence between promoter activation and
131 mRNA accumulation. First, active promoters with very low levels of H3K4me2 are most heavily
132 marked in wildtype testes, regardless of when the genes are expressed. These might be active
133 genes where the histone modification accumulates during the extended growth phase of
134 spermatocytes. Additional examples are the *kumgang* (*kmg*) and *cookie monster* (*comr*) gene
135 promoters which produce mRNA in mid-stage spermatocytes, but are most heavily marked with the
136 H3K4me2 modification in wildtype testes. Second, some promoters acquire the H3K4me2
137 modification well before mRNA accumulates. A small number of genes are expressed in the post-
138 meiotic stages of spermatogenesis, including the "cup" genes (Barreau et al., 2008). Many of these
139 promoters are most heavily marked with the H3K4me2 modification in wildtype testes, but the
140 promoter for *ryder cup* (*r-cup*) is already marked in *aly* mutant testes, implying that it is already
141 active in pre-meiotic stages (**Figure 2B**). Third, as the arrest mutations used here delete most of
142 this gene (*bam*, Bopp et al., 1993) or inactivate it (*aly*, Lin et al., 1996), we cannot measure
143 H3K4me2 modification at these promoters in their arrest genotypes. We note that as these stage-
144 arrest mutations have pleiotropic effects on gene expression (Barreau et al., 2008), some
145 discrepancies between promoter marking in mutants and transcript accumulation in wildtype testes
146 may be due to aberrant transcriptional regulation. Additionally, detection of some changes may be
147 limited since we compare profiles of tissues with diverse cell types.

148 Notably, the importance of the H3K4me2 modification appears to diminish as spermatogenesis
149 proceeds, as the average signal of this mark around promoters for germline-enriched genes in
150 wildtype testes drops in the later stages of spermatogenesis (**Figure 2C**). While the promoters of
151 early germline-expressed genes and somatically-expressed genes have comparable levels of the
152 H3K4me2 modification centered around their TSS, the promoters of late spermatocyte and
153 spermatid genes display very little marking, and this low level extends into gene bodies. This
154 suggests that the activities of H3K4-modifying enzymes are reduced in these later stages.

155 *Profiling FACS-isolated primary spermatocytes*
156 Germline cells undergo massive nuclear expansion and extensive transcriptional activation between
157 mitotic spermatogonia and meiotic division, in part directed by germline-specific variants of general
158 transcription factors (Lim et al., 2012). To specifically profile chromatin features in spermatocytes,
159 we used a spermatocyte-enriched GFP marker to isolate these cells by fluorescence-activated cell
160 sorting (FACS). The *hephaestus* (*heph*) gene encodes an RNA-binding protein that is broadly
161 expressed, but in spermatocytes Heph binds the abundant nuclear transcripts from the *Y*
162 chromosome fertility genes (**Figure 3A**) (Fingerhut et al., 2019). We performed FACS on 40
163 dissociated testes from males carrying a *heph-GFP* transgene, recording the forward scatter (FSC)
164 and GFP signal of each event (**Figure 3B**). FACS profiles from *heph-GFP* samples display a large
165 proportion of events with high GFP signal, which are absent in profiles of wild-type testes. These
166 GFP-labeled spermatocytes have distinct sizes, consistent with the progressive growth of
167 spermatocytes as they approach meiosis (White-Cooper et al., 2010): in a typical FACS
168 experiment, ~5-10% of GFP-positive events have moderate GFP signal and moderate size (Gate
169 1), ~50% of events have very high GFP signal and moderate size (Gate 2), and ~5-10% have high
170 GFP signal and large size (Gate 3). The cells of Gate 3 may represent the latest stage of
171 spermatocytes when heph-GFP signal decreases just before meiosis. Because Gate 2 contained
172 the most GFP-positive events, we focused further analysis on these spermatocytes. We used

173 ~3,000 isolated spermatocytes for each profiling experiment, and since the resulting libraries were
174 comparatively small with high duplication rates, we pooled unique reads from multiple replicates to
175 provide 200,000 – 900,000 unique reads for each profile (**Supplementary Table 1**).

176 We first profiled the distribution of the elongating form of RNA Polymerase II, marked with
177 phosphorylation at Serine-2 (RNAPIIS2p) of the C-terminal tail of the largest subunit of the complex.
178 Inspection of genome landscapes demonstrates the high quality of these profiles. For example, the
179 meiotic beta-tubulin variant gene *betaTub85D* is broadly coated with RNAPIIS2p in isolated
180 spermatocytes, while signal is absent across this gene in somatic cells (**Figure 3C**).

181 Elongating RNAPII is also detectable at many genes that accumulate transcripts in late
182 spermatocytes. For example, 14 genes encoding protamines that package the genome in sperm
183 (Chang et al., 2023) are heavily coated with RNAPII in isolated spermatocytes (**Figure 3E**).
184 Similarly, elongating RNAPII is detectable at genes normally thought to be expressed in post-
185 meiotic cells, such as *heineken-cup* (*h-cup*), implying that RNAPII is engaged at some genes well
186 before their transcripts are detected.
187
188 While these results confirm the cell-type identity of the FACS-isolated cells, we noted that the
189 distribution of RNAPIIS2p across genes such as *betaTub85D* differs from the typical pattern across
190 active genes in somatic cells. Serine-2-phosphorylation of RNAPII is associated with transcriptional
191 elongation, but in Drosophila and in mammalian somatic cells it shows a prominent peak at the 5'
192 end of active genes (Kaya-Okur et al., 2019; Ahmad & Henikoff, 2021). The broad distribution of
193 elongating RNAPII across active genes is typical in spermatocytes. Genes with germline-enriched
194 expression show a broad distribution of elongating RNAPII downstream of their promoters, while
195 somatically expressed genes show a prominent 5' peak (**Figure 3F**).

196 To clearly compare RNAPII distributions between cell-types, we examined long genes that are
197 commonly expressed in both spermatocytes and in wing imaginal discs. One example is the *shuttle*
198 *craft* (*stc*) gene, which is almost 5 kb and is highly expressed. Strikingly, RNAPIIS2p signal at *stc*
199 shows a prominent peak near the promoter in somatic wing imaginal disc cells but is broadly
200 distributed across the gene in spermatocytes (**Figure 3D**). More generally, RNAPIIS2p is broadly
201 distributed across all active genes in spermatocytes, in contrast to the proximally peaked
202 distribution in somatic cells (**Supplementary Figure 2**)

203 The change from peaked to broad distributions of RNAPIIS2p is mirrored in the distributions of the
204 H3K4me2 modification, as this histone modification shows an atypical broad and low distribution
205 across the active *betaTub85D* and *stc* genes in spermatocytes (**Figure 3C,D**). As this histone
206 modification occurs co-transcriptionally, its change in distribution is likely the result of the altered
207 distribution of RNAPII across these genes.

208 *The* X *chromosome is not dosage compensated in spermatocytes*
209 In somatic cells of Drosophila males, the expression of genes on the single *X* chromosome is
210 approximately doubled to equalize expression to autosomal genes. Canonical dosage
211 compensation is accomplished by the Male Specific-Lethal (MSL) RNA-protein complex, which
212 coats the *X* chromosome, catalyzes acetylation of histone H4 at lysine 16, and increases RNAPII
213 density (Akhtar & Becker, 2000). However, in germline cells in the testis cytology detects no

214 enrichment of the H4K16Ac modification, suggesting that *X* chromosome dosage compensation
215 does not occur in this cell type (Rastelli & Kuroda, 1998). Transcriptomic profiling showed that
216 multiple components of the dosage compensation machinery are not expressed in the male
217 germline (Witt et al., 2021). In spite of this, single-cell RNA-seq studies have shown that a perhaps
218 non-canonical form of *X* chromosome dosage compensation occurs in early spermatogonial stages,
219 but disappears by spermatocyte stages (Mahadevaraju et al., 2021; Raz et al., 2023; Witt et al.,
220 2021).

221 The distribution of RNAPII in isolated spermatocytes is consistent with the lack of dosage
222 compensation by this stage of spermatogenesis. Plotting the distribution of RNAPIIS2p across
223 Drosophila chromosomes in wing imaginal discs shows a substantial enrichment across the *X*
224 chromosome, resulting from dosage compensation in these somatic cells (**Figure 4A**). This
225 enrichment of RNAPIIS2p across the *X* chromosome is lost in spermatocytes. To quantify
226 chromosomal changes, we summarized RNAPIIS2p signal for the autosomal *2nd* and *3rd*
227 chromosomes, the quasi-heterochromatic *4th* chromosome, and the sex chromosomes (**Figure**
228 **4B**). As the sex chromosomes are hemizygous, we doubled counts for genes on these
229 chromosomes to calculate polymerase densities per gene copy, and then scaled gene scores to the
230 median value of gene scores on the *2nd* and *3rd* autosomal chromosomes. As expected, the
231 median expression of *X*-linked genes in wing imaginal disc cells is close to twice that of the major
232 autosomes, showing they are dosage compensated. In contrast, median expression from *X*-linked
233 genes is equal to that of the major autosomes in spermatocytes (**Figure 4B**).

234 To assess the chromosomal distribution of the H4K16Ac modification, we profiled it in wing imaginal
235 discs and in isolated spermatocytes. This acetylation is widespread across the genome, consistent
236 with its association with transcriptional activity, and in wing imaginal disc cells it is noticeably
237 enriched across the dosage-compensated *X* chromosome (**Figure 4C**). In stark contrast, the *X*
238 chromosome is depleted for H4K16ac in spermatocytes. Thus, chromatin profiling for both
239 elongating RNAPII and the H4K16ac modification demonstrate there is no dosage compensation of
240 the *X* chromosome in spermatocytes.

241 RNAPII density on the quasi-heterochromatic *4th* chromosome is reduced in spermatocytes,
242 consistent with decreased transcript production from this chromosome in RNA-seq studies
243 (Mahadevaraju et al., 2021; Witt et al., 2021; Raz et al., 2023). The *4th* chromosome is an
244 evolutionary derivative of the *X* chromosome and it has been speculated that it may be subject to
245 similar chromosomal regulation as the *X* (Larsson & Meller, 2006); however, only 10 genes are
246 expressed from this small chromosome in spermatocytes, and this limits any inference about down-
247 regulation of this chromosome. In contrast, the specific activation and accumulation of RNAPIIS2p
248 on *Y* chromosome genes in spermatocytes is dramatic (**Figure 4A,B**). Likewise, the *Y* chromosome
249 becomes conspicuously enriched for the H4K16ac modification in spermatocytes (**Figure 4C**),
250 suggesting this modification is involved in gene activation from this chromosome.

251 *Profiling silencing chromatin marks in spermatocytes*
252 The sex chromosomes of male therian mammals form a cytological sex body in pre-meiotic cells
253 (Solari, 1974). This body is a manifestation of meiotic sex chromosome inactivation (MSCI), where
254 repressive histone modifications silence unpaired chromosomes (Turner, 2015). MSCI has been
255 suggested to occur in the Drosophila male germline to explain the mysterious dominant male

256 sterility of many *X*-to-autosome translocations (Lifschytz & Lindsley, 1972). However, transcriptional
257 profiling of the Drosophila testis has not observed silencing of the *X* chromosome (Mahadevaraju et
258 al., 2021; Witt et al., 2021; Raz et al., 2023). We therefore profiled silencing histone modifications in
259 isolated spermatocytes to determine if molecular marks of MSCI are enriched on the Drosophila *X*
260 chromosome. Methylation of histone H3 at lysine-9 (H3K9me) is generally associated with
261 heterochromatic silencing and marks the precociously silenced *X* chromosome in male mouse
262 spermatogenesis (Khalil et al., 2004; Ernst et al., 2019). In wing imaginal disc cells dimethylation of
263 H3K9 (H3K9me2) is enriched in silenced pericentromeric regions of all chromosomes, as well as
264 throughout the heterochromatic *Y* chromosome and the quasi-heterochromatic *4th* chromosome
265 (**Figure 5A**), consistent with the silencing of repetitive sequence regions in somatic cells. However,
266 the genome in spermatocytes gains the H3K9me2 modification throughout chromosome arms,
267 including those of the major autosomes and the *X* chromosome. In contrast the H3K9me2
268 modification is reduced across the *Y* chromosome, consistent with the activation of *Y*-linked genes
269 in this cell type (**Figure 5A**). Although the H3K9me2 mark is reduced across this chromosome and
270 across pericentromeric regions, substantial chromosomal methylation remains in spermatocytes.

271 A major system of chromatin repression uses trimethylation of histone H3 at lysine-27 (H3K27me3)
272 to direct developmental gene silencing (Grossniklaus & Paro, 2014). Although this mark is not
273 associated with MSCI in mammals (Mu et al., 2014), we profiled it in Drosophila spermatocytes.
274 There is little change in the chromosomal distribution of the H3K27me3 modification between wing
275 imaginal disc cells and spermatocytes (**Figure 5B**). There is a slight apparent reduction of this
276 modification across the *X* chromosome and a slight gain across the *Y* chromosome, but these
277 differences may be due to the developmental lineages of these two samples. Overall, the constancy
278 of chromosomal patterns of the H3K27me3 modification is consistent with the inactivation of the
279 histone methyltransferase *Enhancer of zeste* (*E(z)*) in spermatocytes (Chen et al., 2011).

280 *Mono-ubiquitinylation of histone H2A marks the active* Y *chromosome*
281 An additional histone modification associated with precocious silencing of the *X* chromosome in
282 male mammals is the mono-ubiquitinylation of histone H2A at lysine-119 (uH2A) (Baarends et al.,
283 1999). This modification is conserved at the homologous lysine-118 position of Drosophila histone
284 H2A, and is linked to Polycomb-mediated silencing across eukaryotes (Barbour et al., 2020). We
285 therefore profiled the distribution of the uH2A modification in wing imaginal discs and in isolated
286 spermatocytes to determine if this modification marked the *X* chromosome. The uH2A mark is
287 broadly enriched throughout the arms of autosomes in both cell types, but shows no enrichment
288 across the *X* chromosome in spermatocytes (**Figure 6A**). Thus, this chromatin marker of
289 mammalian MSCI is also absent from the Drosophila *X* chromosome. However, the active *Y*
290 chromosome is strikingly enriched for the uH2A modification in spermatocytes, with additional
291 moderate enrichment in the repetitive pericentromeric regions of all chromosomes (**Figure 6A**).

292 We confirmed the chromosomal enrichment of the uH2A modification by immunostaining
293 spermatocytes (**Figure 6B**). The subnuclear pattern of a Polycomb-GFP (PcGFP) fusion protein
294 distinguishes early from late spermatocytes (Dietzel et al., 1999; El-Sharnouby et al., 2013). Using
295 this marker, we see that uH2A is largely absent from the nucleus of early spermatocytes. In mid-
296 stage spermatocytes a stringy wedge of uH2A staining appears in the interchromosomal space
297 between the chromatin bodies and expands to one or two wedges in late spermatocytes (**Figure**

298 **6B**). The timing of appearance and position of these stained bodies resemble that of the
299 chromosome loops that unfold from *Y*-linked genes as they are expressed (Bonaccorsi et al., 1988).
300 We therefore engineered *XO* male flies lacking a *Y* chromosome and immunostained their
301 spermatocytes. The uH2A modification is present in these cells, but with a distinctly different focal
302 appearance, suggesting that the ubiquitinylated histone aggregates in spermatocytes without a *Y*
303 chromosome (**Figure 6B**). To confirm the timing of the appearance of the uH2A body, we
304 immunostained germline nuclei from *bam* and *aly* stage-arrest mutants. The spermatogonial nuclei
305 from *bam* mutant testes lack uH2A staining, while early spermatocyte nuclei from *aly* mutant testes
306 have only a small uH2A body that always abuts against the nucleolus (**Figure 6B**). Thus, the uH2A
307 body accumulates during the early spermatocyte stage and expands as spermatocytes develop.
308 The timing and position of the uH2A body is consistent with the idea that it contains the *Y*
309 chromosome, which is transcriptionally active in these stages.

310 To further characterize the relationship between transcriptional activity of the *Y* chromosome and
311 the uH2A modification, we plotted signal for the uH2A modification and for RNAPIIS2p at *Y*-linked
312 gene promoters (**Figure 6C**). In wing imaginal discs these promoters have little RNAPIIS2p or
313 uH2A modification, but there is strong relative enrichment for both features at these promoters in
314 spermatocytes, consistent with transcriptional activity of the *Y* chromosome. Since the uH2A
315 modification also becomes enriched in pericentromeric regions, we compared the enrichment of the
316 uH2A modification and RNAPIIS2p at repetitive transposons that constitute a large fraction of these
317 regions. A number of transposons gain RNAPIIS2p signal specifically in spermatocytes (**Figure 6D**;
318 **Supplementary Table 4**; **Supplementary Figure 3**), consistent with their transcriptional activation
319 (Lawlor et al., 2021). These activated transposons also gain the uH2A modification. These
320 correspondences suggest that the uH2A modification contributes to transcriptional activation of
321 heterochromatic regions in spermatocytes.

322 **Discussion**

323 Germline cells use distinctive variations on transcriptional gene regulation, and studies of
324 Drosophila spermatogenesis have detailed many specialized alterations of core general
325 transcription factors that direct expression programs as differentiation proceeds (Hiller et al., 2004).
326 However, the chromatin features of gene regulation in spermatogenesis have been less thoroughly
327 characterized, in part because of the complexity of the tissue and limiting numbers of germline cells.
328 We have addressed this by performing efficient CUT&Tag chromatin profiling for both active and
329 repressive chromatin marks in the Drosophila testis and in isolated spermatocytes. These profiles
330 reveal several notable features of the epigenome in the differentiating germline. First, integration of
331 chromatin marks with published gene expression data details a general correspondence between
332 gene promoter activation and mRNA production as expected, but for a fraction of genes their
333 promoters activate earlier than expected. Second, genes that are activated late in spermatogenesis
334 tend to have very reduced active chromatin marks at their promoters. Third, while many active
335 genes in somatic cells accumulate RNA polymerase II near their gene starts, such accumulation is
336 absent in spermatocytes. Fourth, integration of chromatin profiling for multiple chromatin marks and
337 profiling of RNA polymerase II demonstrate that the single *X* chromosome is neither dosage
338 compensated nor globally inactivated in spermatocytes. Finally, histone H2A mono-ubiquitinylation
339 appears to have a specialized role in activation of the heterochromatic *Y* chromosome.

340 *Quirks of gene expression in the male germline*
341 The uniform distribution of RNAPII throughout active genes in male germline cells is strikingly
342 different from the typical accumulation of RNAPII near promoters in somatic cells. Promoter-
343 proximal accumulation results from dynamic pausing of RNAPII before conversion into the
344 productive elongating isoform, and is a major control point for transcriptional regulation in somatic
345 cells (Muniz et al., 2021). Thus, the uniformity of RNAPII across expressed genes in spermatocytes
346 suggests that pausing does not occur, necessitating gene regulation solely by transcription factor
347 and RNAPII recruitment. This may allow for a simpler promoter architecture, and indeed
348 spermatogenic gene promoters are distinctively small (White-Cooper et al., 2010). Alternatively,
349 RNAPII progression through gene bodies may be slow, altering the steady-state distribution of
350 elongating polymerase. Further, either of these changes in RNAPII behavior would affect chromatin
351 features of active genes. RNAPII binds enzymes that progressively methylate the lysine-4 residue
352 of histone H3, and so active promoters in somatic cells are typically marked with both H3K4-
353 dimethylation and -trimethylation (Bernstein et al., 2005). A consequence of chaning the rate of
354 polymerase progression in spermatocytes would be reduced methylation of active promoters (which
355 we observe is most severe in late spermatocyte and post-meiotic stages), and thereby reduced
356 reliance of these marks for promoting transcription.

357 *The* X *chromosome is neither dosage-compensated nor inactivated in spermatocytes*
358 While protein and lncRNA components of the somatic dosage compensation machinery are not
359 produced in the male germline, transcriptional profiling described up-regulation of the single *X*
360 chromosome in early germline stages (Mahadevaraju et al., 2021; Witt et al., 2021). The
361 mechanism for this non-canonical dosage compensation remains unknown (Witt et al., 2021), but
362 by the spermatocyte stage *X*-linked genes are no longer up-regulated. Our profiling of RNAPII
363 confirms that there is no up-regulation of this chromosome in spermatocytes. There has been
364 substantial investigation into whether the *X* is inactivated in spermatocytes, inspired by the
365 regulation of sex chromosomes in mammals (Vibranovski, 2014; Turner, 2015) and the moderate
366 depletion of male-germline-expressed genes on the Drosophila *X* chromosome (Parisi et al., 2003).
367 In mammalian male germlines the *X* and *Y* chromosomes undergo Meiotic Sex Chromosome
368 Inactivation (MSCI), where these chromosomes are precociously silenced just before meiosis
369 (Turner, 2015). A variety of chromatin features accumulate across the sex chromosomes at this
370 time, including the enrichment of both H3K9me2 and uH2A histone modifications. However, we find
371 that neither of these histone modifications is enriched on the *X* chromosome in the Drosophila male
372 germline. This, combined with the equivalent amounts of RNA polymerase II on *X*-linked genes and
373 autosomal ones implies that there is no *X* chromosome inactivation in Drosophila.

374 Why do flies differ from mammals? Mammalian MSCI is considered to be an elaborated response
375 of germline cells to the detection of the unpaired sex chromosomes (Huynh & Lee, 2005). However,
376 meiosis in Drosophila males is unusual in that all the chromosomes do not synapse nor recombine
377 (McKee & Handel, 1993). Logically, the evolutionary loss of synapsis must have required the
378 concomitant loss of an unpaired chromosome response in Drosophila males. Indeed, many of the
379 proteins recruited to the mammalian sex body are normally involved in meiotic recombination but
380 have been repurposed for unpaired chromosome inactivation (Abe et al., 2022), supporting the idea
381 that MSCI is mechanistically linked to synapsis. Alternatively, mammalian MSCI may be a variant of
382 the X-inactivation system that operates in females for dosage compensation (Huynh & Lee, 2005)

383 but since Drosophila solved the dosage compensation problem without inactivation, this precluded
384 the evolution of MSCI. These possibilities are not mutually exclusive.

385 *Activation of the* Y *chromosome*
386 The *Y* chromosome in Drosophila is unique in that it is almost entirely composed of repetitive
387 sequence, but also carries some unique genes required for male fertility (Chang & Larracuente,
388 2019). Thus, in somatic cell types this a heterochromatic chromosome, but is heavily transcribed in
389 spermatocytes (Bonaccorsi et al., 1988). This activated chromosome accumulates multiple histone
390 modifications (Hennig & Weyrich, 2013), some of which we have profiled here. Surprisingly, one of
391 the histone modifications that coats the activated *Y* chromosome is mono-ubiquitinylation of histone
392 H2A modification. This modification is typically associated with Polycomb-mediated gene silencing
393 in somatic cells (Aloia et al., 2013), where it is catalyzed by the Sce/RING1B enzyme subunit of the
394 Polycomb Repressive Complex 1 (PRC1) (Gorfinkiel et al., 2004; Wang et al., 2004). However, the
395 Polycomb subunit of PRC1 does not co-localize with the uH2A-coated *Y* chromosome in
396 spermatocytes, suggesting that it is not catalyzed by Sce here. Indeed, uH2A also coats the *X* and
397 *Y* chromosomes in mammalian spermatocytes, where this modification is catalyzed by a distinct
398 enzyme, the UBR2 E3 ubiquitin ligase (An et al., 2010). The Drosophila genome encodes a
399 homolog of this protein family, as well as many other ubiquitin ligases, some of which target the
400 H2A histone (Tasaki et al., 2005). We do not know which enzyme is responsible for the uH2A
401 modification in the Drosophila male germline, although some candidates have male sterile
402 phenotypes when mutated (Rathke et al., 2007). While it is surprising to find a histone modification
403 conventionally associated with silencing enriched on an activated chromosome (and indeed the
404 reason we profiled it was as a putative MSCI marker), the roles of uH2A in gene regulation are
405 diverse even in somatic cells. The uH2A modification is associated with both silenced and some
406 active genes in developing eye tissue (Loubiere et al., 2020), and counters chromatin compaction in
407 the early embryo (Bonnet et al., 2022). In addition to the *Y* chromosome, a number of
408 heterochromatic transposons in the Drosophila male germline are also activated and accumulate
409 the uH2A modification. Thus, it is conceivable that this modification – perhaps in combination with
410 other marks – works generally to modulate transcription of extremely heterochromatic regions in
411 spermatocytes.

412 **Methods**
413 *Fly strains*
414 All crosses were performed at 25˚C. All mutations and chromosomal rearrangements used here are
415 described in Flybase (http://www.flybase.org). The w^{1118} strain was used as a wildtype control. The
416 *heph-GFP* males used for profiling have the genotype *y w/Y ; P[PTT-GC]heph*^{CC00664}*/TM3, Ser Sb*.
417 The *bam* mutant males have the genotype *w/Y ; e bam*^{D86}*/Df(3R)FDD-0089346*. The *aly* mutant
418 males have the genotype *P[ry11]ry2, mwh aly*^{1} *ry*^{506} *e/Df(3L)BSC428*. Additional genotypes used for
419 cytological characterization were *y w P[bam-GAL4:VP16,w*$^{+}$*]1/Y ; P[UAS-RFP,w*$^{+}$*]2/2 ; P[PTT-*
420 *GC]heph*^{CC00664}*/3* and w^{1118}*/Y ; P[Pc-eGFP,w*$^{+}$*]3*.

421 *Antibodies*
422 The following antibodies were used: Epicypher 13-0027 anti-H3-K4-dimethyl, Cell Signalling
423 Technology E1Z3G anti-RNAPII-Serine-2-phosphorylation, Cell Signalling Technology 8240 anti-
424 H2A-K119-ubiquitinylation, EMD Millipore 05-1249 anti-H3-K9-dimethyl, Cell Signalling Technology

425 C36B11 anti-H3-K27-trimethyl, Abcam ab109463 anti-H4-K16-acetyl, and Abcam ab5821 anti-
426 fibrillarin.
427
428 *Imaging whole testes*
429 Testes from one-day old adult males were dissected and fixed in 4% formaldehyde/PBS with 0.1%
430 Triton-X100 (PBST) for 10 minutes, stained with 0.5 µg/mL DAPI/PBS, and mounted in 80%
431 glycerol on slides. Testes were imaged by epifluorescence on an EVOS FL Auto 2 inverted
432 microscope (Thermo Fisher Scientific) with a 10X objective.

433 *Imaging spermatocytes*
434 Testes from third-instar male larvae were prepared as described [Bonaccorsi *et al*, 2000]. Briefly,
435 one testis was dissected in a drop of PBS on a Histobond glass slide (VWR 16004-406), squashed
436 gently with a RainX (ITW Global Brands) coated coverslip, then flash-frozen in liquid nitrogen. After
437 popping off the coverslip, the sample was fixed with 4% formaldehyde/PBST for 5 minutes, and
438 incubated with 0.3% sodium deoxycholate/PBST twice for 20 minutes each. Samples were
439 incubated with primary antiserum in PBST supplemented with 0.1% bovine serum albumin (BSA) at
440 4˚ overnight, and finally with fluorescently-labeled secondary antibodies (1:200 dilution, Jackson
441 ImmunoResearch). Slides were stained with 0.5 µg/mL DAPI/PBS, mounted in 80% glycerol, and
442 imaged by epifluorescence on an EVOS FL Auto 2 inverted microscope (Thermo Fisher Scientific)
443 with a 40X objective. Dissection and immunostaining was typically repeated at least 10 times to
444 confirm results. We also imaged stained spermatocytes from adult testes, but imaging of larval
445 spermatocytes was typically cleaner with less background. Pseudo-colored images were adjusted
446 and composited in Adobe Photoshop and Adobe Illustrator.

447 *Whole-mount CUT&Tag*
448 To perform CUT&Tag [6] for whole tissues ("whole-mount CUT&Tag"), we dissected 10 testes from
449 one-day-old adults or 10 imaginal wing discs from 3rd instar larvae in PBS buffer supplemented
450 with cOmplete protease inhibitor (Roche 11697498001). Dissected tissues were permeabilized with
451 0.1% Triton/PBS for 30 minutes at room temperature, and then manually transferred into the
452 following CUT&Tag solutions sequentially between wells of a glass dissection plate: primary
453 antibody solution (diluted in Wash+ buffer (20 mM HEPES pH 7.5, 150 mM NaCl, 0.5 mM
454 spermidine, 2 mM EDTA, 1% BSA, with cOmplete protease inhibitor)) overnight at 4˚, secondary
455 antibody solution (in Wash+ buffer) for 1 hour at room temperature, and then incubated with loaded
456 protein-A-Tn5 (in 300Wash+ buffer (20 mM HEPES pH 7.5, 300 mM NaCl, 0.5 mM spermidine with
457 cOmplete protease inhibitor) for 1 hour. After one wash with 300Wash+ buffer, samples were
458 incubated in 300Wash+ buffer supplemented with 10 mM MgCl2 for 1 hour at 37˚ to tagment
459 chromatin. Tissues were then dissociated with collagenase (2 mg/mL, Sigma C9407) in HEPESCA
460 (50mM HEPES buffer pH 7.5, 360 µM $CaCl_2$) solution at 37˚ for 1 hour. We then added SDS to
461 0.16%, protease K to 0.3 mg/mL, and EDTA to 16 mM and incubated at 58˚ for 1 hour, and DNA
462 was purified by phenol:chloroform extraction and ethanol precipitation. Libraries were prepared as
463 described (Kaya-Okur et al., 2019) (https://www.protocols.io/view/bench-top-cut-amp-tag-
464 kqdg34qdpl25/v3), with 14 cycles of PCR. Libraries were sequenced in PE50 mode on the Illumina
465 NextSeq 2000 platform at the Fred Hutchinson Cancer Center Genomics Shared Resource.

466 *FACS-CUT&Tag of spermatocytes*

467 40 testes were dissected from one-day old adult *heph-GFP* males and digested in 200 µL of 2
468 mg/mL collagenase (Sigma C9407) in HEPESCA solution at 37˚ for one hour. The sample was then
469 repeatedly pipetted with a P200 pipette tip to dissociate the tissue, then passed through a 35 µM
470 filter with 5 mL collection tube (Corning 352235) on ice. The filter was washed with PBS to bring the
471 total volume of collected filtrate to 1 mL. A Sony MA900 Multi-Application Cell Sorter with a 100 µM
472 nozzle, flow pressure of 2, GFP laser settings of 32% and FSC=1 was used for isolating cells.
473 Isolated cells were collected in 1 mL of PBS in 5 mL tubes. Benchtop CUT&Tag was performed on
474 these samples as described [Kaya-Okur *et al*, 2019], and sequenced in PE50 paired-end mode.

475 *Genome mapping*
476 To streamline analysis of repetitive transposons in the fly genome, we used a modified version of
477 the release r6.30 *D. melanogaster* genome for mapping where repetitive sequences are masked
478 out of the genome (http://hgdownload.cse.ucsc.edu/goldenPath/dm6/bigZips/dm6.fa.masked.gz)
479 and with consensus sequences for 128 transposon sequences
480 (https://github.com/bergmanlab/drosophila-
481 transposons/blob/master/misc/D_mel_transposon_sequence_set.fa) appended [Ashburner *et al*,
482 2021]. Paired-end reads were mapped to this assembly using Bowtie2 (using parameters, e.g.: --
483 end-to-end --very-sensitive --no-mixed --no-discordant -q --phred33 -I 10 -X 700).

484 Mapped reads from whole-tissue replicates were merged using samtools-merge and converted to
485 coverage tracks using bedtools-genomecov with options -scale -fs. For profiling FACS-isolated
486 spermatocytes, duplicate reads were removed from each library using Picard-remove duplicates,
487 and then replicates were merged using samtools-merge and converted to coverage tracks using
488 bedtools-genomecov with options -scale -fs. These tracks are hosted at UCSC
489 (https://genome.ucsc.edu/s/jamesanderson12358/analysis230508___UCSC_session_germline_MS
490) for visualization, and selected regions were exported as PDF files.

491 *Processing of FCA testis snRNA-seq data*
492 We downloaded snRNA-seq data generated by the Fly Cell Atlas project (Li et al., 2022) as a
493 Seurat object linked in supplementary data of (Raz et al., 2023), summarizing gene expression data
494 of single nuclei from dissociated Drosophila adult testes. We used the Seurat function
495 AverageExpression() to get the average expression of all genes in each of 40 UMAP groups which
496 represent distinct cell types of the testis. This produced a 40 groups x 15,833 genes table.
497 The 18 germline groups and 22 somatic groups assigned in (Raz et al., 2023) are:

498 1. Spermatogonium
499 2. spermatogonium-spermatocyte transition
500 3. mid-late proliferating spermatogonia
501 4. spermatocyte 0
502 5. spermatocyte 1
503 6. spermatocyte 2
504 7. spermatocyte 3
505 8. spermatocyte 4
506 9. spermatocyte 5
507 10. spermatocyte 6
508 11. spermatocyte 7a

12. maturing primary spermatocyte
13. spermatocyte
14. late primary spermatocyte
15. early elongation stage spermatid
16. early-mid elongation-stage spermatid
17. mid-late elongation-stage spermatid
18. spermatid
19. hub
20. cyst stem cell
21. early cyst cell 1
22. early cyst cell 2
23. cyst cell intermediate
24. spermatocyte cyst cell branch a
25. spermatocyte cyst cell branch b
26. cyst cell branch a
27. cyst cell branch b
28. male gonad associated epithelium
29. seminal vesicle
30. adult tracheocyte
31. muscle cell
32. testis epithelium
33. hemocyte
34. hcc
35. tcc
36. pigment cell
37. adult fat body
38. secretory cell of the male reproductive tract
39. adult neuron
40. “Unannotated”

Promoter and gene scoring tables

We compiled a list of genes with male-germline-enriched expression as follows. We compiled a list of unique protein-coding mRNAs and lncRNA genes from the Drosophila dmel_r6.31 genome assembly (http://ftp.flybase.net/releases/FB2019_06/dmel_r6.31/gtf/), and matched FCA expression data for 40 testis cell types [Raz 2023] to each gene with a lookup table. There were 1,062 genes that are not represented in the expression dataset; these genes are listed with #N/A values for gene expression.

For each gene, we calculated its average expression in the 18 germline groups (gexp) and its average expression in 21 somatic groups (sexp). The 40th ‘unannotated’ group was not considered for gexp or sexp values. We then used k-means clustering (k=10) to group genes by cell-type expression within the testis (**Supplementary Figure 1**). The k-means groups 1-5 were associated with gene expression in germline clusters 1-18. The remaining groups 6-10 were associated with

552 gene expression in somatic clusters 19-40, and we collapsed these into one somatic group called
553 “all somatic categories” (k-cluster group 11). We added these k-cluster annotations to each gene.
554
555 We then selected 6,419 genes with $\log_2$Fold-change$\geq$1 average expression in germline groups than
556 in testis somatic groups (termed genes with germline-enriched expression). This table is included
557 as **Supplementary Table 3**. To assign alternative promoters to each gene, for each transcript in
558 the .gtf file with orientation “+” we assigned the minimum coordinate as its TSS position, and for
559 each transcript with orientation “-“ we assigned the maximum coordinate as its TSS position. We
560 retained only one instance of duplicate TSSs for genes with TSS coordinates represented multiple
561 times. In 144 instances two gene names share the same TSS coordinate, and we retained a TSS
562 for each gene in the table. This table of 21,982 promoters is included as **Supplementary Table 2**.
563
564 For each gene, we determined the identity and distance to the nearest promoter of the next
565 upstream gene using the bedtools/closest with parameters: -D a -fu , and for the next downstream
566 gene with parameters: -D a -fd .

567 To summarize the enrichment of chromatin marks at promoters, we counted mapped reads in an
568 interval from -200 – +500 bp around each TSS in merged profiling data by summing reads using
569 deeptools/multiBamSummary with parameters: BED-file –BED

570 and scaled counts by the number of reads in each library (counts * 1,000,000) / (number of reads in
571 library) to give Counts per Million (CPM). Profiling counts were transformed into z-scores for each
572 promoter between *bam*, *aly*, and wildtype testis samples, and these values are appended to
573 **Supplementary Table 2**.

574 To summarize the enrichment of chromatin marks across genes, we counted mapped reads from
575 the start to the end of each gene in merged profiling data by summing reads using
576 deeptools/multiBamSummary with parameters: BED-file –BED

577 and scaled counts by the number of reads in each library and the length of the gene (counts *
578 1,000,000) / (number of reads in library * gene length in kb) to give Counts per Kilobase per Million
579 (CPKM), and these values are appended to **Supplementary Table 3**.

580 To summarize enrichment of chromatin marks across transposons, we counted mapped reads
581 across consensus transposon sequences using deeptools/multiBamSummary with parameters:
582 BED-file –BED

583 and scaled counts as CPKM. These values are provided in **Supplementary Table 4**.

584 *Genomic display*
585 For average plots of H3K4me2 signal around promoters, profiling coverage was summarized with
586 deepTools/bamCoverage $\pm$1 kb around annotated TSSs excluding regions with a second gene
587 promoter in the display window with 10 bp binning, and plotted using plotHeatmap.
588
589 For average plots of H3K4me2 signal around promoters, profiling coverage was summarized with
590 deepTools/bamCoverage $\pm$1 kb around annotated TSSs excluding regions with a second gene
591 promoter in the display window with 10 bp binning, and plotted using plotHeatmap.

592
593 For heatmapping of RNAPIIS2p signal at gene starts, we used deepTools/computeMatrix with
594 parameters: -b 2000 -a 2000 -R and then we used deepTools/plotHeatmap with parameters: --
595 colorMap viridis.
596
597 For visualizing the chromosomal distribution of CUT&Tag data as CIRCOS plots, we used the
598 circlize package in R with default settings (circlize version 0.4.15). Genome coverage files for
599 plotting were generated by deepTools/bamCoverage command, using parameters:

600 -bs 20000 --centerReads --effectiveGenomeSize 142573017 -of bedgraph

601 And plotted in consecutive 20 kb bins. The innermost 3 rings of each plot display genomic
602 coverage, with color-coding set independently per ring.The color of bins in the outer ring correspond
603 to the fold-change of signal in spermatocytes compared to wing imaginal discs calculated using
604 deepTools/multiBigwigSummary command, with parameters:

605 bins -bs 20000 –outRawCounts

606 For boxplots, the enrichment score for each gene was scaled by dividing its read count by the
607 median count in the "chromosome *2* & *3*" category and plotted, discarding genes with enrichment
608 score = 0 in either dissociated testes, in spermatocytes, or in wing imaginal discs.

609

610 **Data availability**

611 Data generated in this study is deposited in GEO under accession GSE225300.

612

613 **Funding**

614 National Institutes of Health NHGRI R01 HG010492 (S. Henikoff) and Howard Hughes Medical
615 Institute (S. Henikoff).

616

617 **Figure Legends**

618 **Figure 1. Profiling of the histone H3K4me2 modification in the Drosophila testis.**
619 (**A**) Schematic of male germline stages in Drosophila. Germline stem cells (GSCs, fuschia) are
620 located in the apical tip of the testis. After an asymmetric division a progeny spermatogonium
621 (purple) undergoes 4 rounds of mitotic divisions. After one last S phase cells grow over ~3 days as
622 spermatocytes (blue, light green, dark green) before meiosis (red). Post-meiotic differentiation
623 produces mature sperm (black) with elongated nuclei. Somatic cell types of the testis are not
624 shown.
625 (**B-E**) Distribution of the H3K4me2 modification in testes from *bam* mutants, from *aly* mutants, from
626 wildtype animals, and from wing imaginal discs.

627 (**B**) H3K4me2 around the GSC-expressed *nanos* gene. Neighboring genes show peaks in all
628 samples, while low signal across *nanos* is highest in testes from *bam* mutants, and apparent in all
629 three testes samples.
630 (**C**) H3K4me2 around the spermatocyte-expressed *loopin-1* gene. H3K4me2 signal appears in *aly*
631 mutant samples (which contain early spermatocytes) and reach high levels in wildtype testes (which
632 include later stages of spermatogenesis).
633 (**D**) H3K4me2 around the meiotically-expressed genes *Mst36Fa* and *Mst36Fb* genes. Signal across
634 these genes only appears in wildtype testes.
635 (**E**) H3K4me2 around the *abd-A* and *Abd-B* genes, which are expressed in somatic cells of the
636 testis.
637
638 **Figure 2. Changes in the histone H3K4me2 modification in germline-expressed genes.**
639 H3K4me2 signal around gene promoters (-200–+500 bp) with transcripts enriched in specific
640 germline cell types. Transcript expression was derived from FCA snRNA-seq clustering [Raz *et al*,
641 2023].
642 (**A**) Expression (snRNA-seq) in wildtype testes and H3K4me2 enrichment in *bam* mutant, in *aly*
643 mutant, and in wildtype testes in germline stages. Z-scores for H3K4me2 signal were calculated
644 between the three genotypes. Notable germline-enriched genes are indicated, including those
645 expressed in GSCs, in meiosis, or for cell division (black), linked to the *Y* chromosome (purple), or
646 expressed post-meiotically (orange).
647 (**B**) Selected examples of promoters with germline-enriched expression. Expression z-scores from
648 FCA snRNA-seq across 18 germline clusters (Raz et al. 2023) and H3K4me2 enrichment in *bam*
649 mutant, in *aly* mutant, and in wildtype testes.
650 (**C**) Distribution of H3K4me2 around promoters with germline-enriched expression. The testis
651 somatic category comprises the top tercile of promoters with somatic cell-type expression in
652 snRNA-seq data (Raz et al. 2023). Only promoters with no promoter of a second gene within 1 kb
653 upstream are shown.
654
655 **Figure 3. Profiling RNA Polymerase II in isolated spermatocytes.**
656 (**A**) An adult testis carrying a *UASRFP* construct induced by a *bamGAL4* driver and a *hephGFP*
657 construct. Gonial cells are labeled red while spermatocytes are labeled green with fluorescent
658 proteins.
659 **(B)** FACS plots of recorded events from dissociated testes for forward scatter (FSC) and GFP
660 signal. Boxes indicate events collected for chromatin profiling.
661 **(C)** Distribution of RNAPIIS2p at the spermatocyte-expressed *betaTub85D* gene in isolated
662 spermatocytes and in wing imaginal discs.
663 **(D)** Distribution of RNAPIIS2p at the broadly-expressed *stc* gene in isolated spermatocytes and in
664 wing imaginal discs. RNAPIIS2p is strongly localized at the *stc* promoter in wing imaginal discs, but
665 more evenly distributed in spermatocytes.
666 (**E**) Selected examples of genes with late germline expression and for protamines. Expression z-
667 scores from FCA snRNA-seq across 18 germline clusters (Raz *et al.*, 2023) and RNAPIIS2p
668 enrichment in isolated spermatocytes.
669 (**F**) Enrichment of RNAPIIS2p in isolated spermatocytes and in wing imaginal discs across genes
670 with germline-enriched transcripts.

671
672 **Figure 4. Chromosomal distribution of RNA polymerase II and H4K16ac in isolated**
673 **spermatocytes.**
674 (**A**) CIRCOS plot of RNAPIIS2p across Drosophila chromosomes. The signal (black) in IgG
675 controls, in wing imaginal discs, and in isolated spermatocytes is shown in internal rings, and the
676 log2 fold-change of signals between spermatocytes and wings is shown in the outer ring.
677 (**B**) Enrichment of RNAPIIs2p across gene bodies in wing imaginal discs, in whole dissociated
678 testes, and in isolated spermatocytes separated by chromosomal location. Scores are scaled to the
679 median score on the 2nd and 3rd chromosomes.
680 (**C**) CIRCOS plot of the dosage-compensation marker histone H4K16ac across Drosophila
681 chromosomes. Signal (black) in IgG controls, in wing imaginal discs, and in isolated spermatocytes
682 is shown in internal rings, and the log2 fold-change of signals between spermatocytes and wings is
683 shown in the outer ring.
684
685 **Figure 5. Chromosomal distribution of repressive histone modifications in isolated**
686 **spermatocytes.** CIRCOS plots across Drosophila chromosomes show signal (black) in IgG
687 controls, in wing imaginal discs, and in isolated spermatocytes in internal rings, and the log2 fold-
688 change of signals between spermatocytes and wings in the outer ring.
689 (**A**) Distribution of the heterochromatin-silencing marker H3K9me2.
690 (**B**) Distribution of the Polycomb-silencing marker H3K27me3.
691
692 **Figure 6. Chromosomal distribution of ubiquitinylated histone H2A in isolated**
693 **spermatocytes.**
694 (**A**) CIRCOS plots of uH2A across Drosophila chromosomes in IgG controls, in wing imaginal discs,
695 and in isolated spermatocytes.
696 (**B**) Immunostaining of uHA (blue) and the nucleolar marker fibrillarin (red) on germline nuclei.
697 Early-, mid-, and late-spermatocyte stage were identified by PcGFP (green) localization pattern in
698 wildtype spermatocytes and in *X/O* spermatocytes. Testes from *bam* mutants contain gonial cells,
699 while testes from *aly* mutants contain mostly early spermatocytes.
700 (**C**) Correspondence of uH2A and RNAPIIS2p signals around the promoters of genes on the *Y*
701 chromosome in wing imaginal discs and in isolated spermatocytes.
702 (**D**) Correspondence of uH2A and RNAPIIS2p signals across transposon consensus sequences in
703 wing imaginal discs and in isolated spermatocytes.
704

705 **References**

706 Abe, H., Yeh, Y. H., Munakata, Y., Ishiguro, K. I., Andreassen, P. R., & Namekawa, S. H.
707 (2022). Active DNA damage response signaling initiates and maintains meiotic sex
708 chromosome inactivation. *Nat Commun*, *13*(1), 7212. https://doi.org/10.1038/s41467-022-
709 34295-5 PMC9705562
710 Ahmad, K., & Henikoff, S. (2021). The H3.3K27M oncohistone antagonizes reprogramming in
711 Drosophila. *PLoS Genet*, *17*(7), e1009225. https://doi.org/10.1371/journal.pgen.1009225
712 PMC8320987

Akhtar, A., & Becker, P. B. (2000). Activation of transcription through histone H4 acetylation by MOF, an acetyltransferase essential for dosage compensation in Drosophila. *Mol Cell*, *5*(2), 367-375. https://doi.org/10.1016/s1097-2765(00)80431-1

Aloia, L., Di Stefano, B., & Di Croce, L. (2013). Polycomb complexes in stem cells and embryonic development. *Development*, *140*(12), 2525-2534. https://doi.org/10.1242/dev.091553

An, J. Y., Kim, E. A., Jiang, Y., Zakrzewska, A., Kim, D. E., Lee, M. J., Mook-Jung, I., Zhang, Y., & Kwon, Y. T. (2010). UBR2 mediates transcriptional silencing during spermatogenesis via histone ubiquitination. *Proc Natl Acad Sci U S A*, *107*(5), 1912-1917. https://doi.org/10.1073/pnas.0910267107 PMC2836623

Ashburner, M., Bayraktaroglu, L., Benos, T., Chillemi, J., Crosby, L., de Grey, A., Han, S., Kaminker, J., Lewis, S., Liao, G., Reese, M., & Bergman, C. (2021). Drosophila transposon canonical sequences (Version 10.2) [Data set]. https://github.com/bergmanlab/drosophila-transposons/

Baarends, W. M., Hoogerbrugge, J. W., Roest, H. P., Ooms, M., Vreeburg, J., Hoeijmakers, J. H., & Grootegoed, J. A. (1999). Histone ubiquitination and chromatin remodeling in mouse spermatogenesis. *Dev Biol*, *207*(2), 322-333. https://doi.org/10.1006/dbio.1998.9155

Barbour, H., Daou, S., Hendzel, M., & Affar, E. B. (2020). Polycomb group-mediated histone H2A monoubiquitination in epigenome regulation and nuclear processes. *Nat Commun*, *11*(1), 5947. https://doi.org/10.1038/s41467-020-19722-9 PMC7683540

Barreau, C., Benson, E., Gudmannsdottir, E., Newton, F., & White-Cooper, H. (2008). Post-meiotic transcription in Drosophila testes. *Development*, *135*(11), 1897-1902. https://doi.org/10.1242/dev.021949

Bernstein, B. E., Kamal, M., Lindblad-Toh, K., Bekiranov, S., Bailey, D. K., Huebert, D. J., McMahon, S., Karlsson, E. K., Kulbokas, E. J., 3rd, Gingeras, T. R., Schreiber, S. L., & Lander, E. S. (2005). Genomic maps and comparative analysis of histone modifications in human and mouse. *Cell*, *120*(2), 169-181. https://doi.org/10.1016/j.cell.2005.01.001

Bonaccorsi, S., Pisano, C., Puoti, F., & Gatti, M. (1988). Y chromosome loops in Drosophila melanogaster. *Genetics*, *120*(4), 1015-1034. https://doi.org/10.1093/genetics/120.4.1015 PMC1203565

Bonaccorsi, S., Giansanti, M.G., Cenci, G., & Gatti, M. “Chromatin Staining of Drosophila Testes.” Adapted from *Drosophila Protocols* (ed. Sullivan et al.). CSHL Press, Cold Spring Harbor, NY, USA, 2000. doi:10.1101/pdb.prot067363.

Bonnet, J., Boichenko, I., Kalb, R., Le Jeune, M., Maltseva, S., Pieropan, M., Finkl, K., Fierz, B., & Müller, J. (2022). PR-DUB preserves Polycomb repression by preventing excessive accumulation of H2Aub1, an antagonist of chromatin compaction. *Genes Dev*, *36*(19-20), 1046-1061. https://doi.org/10.1101/gad.350014.122 PMC9744231

Bopp, D., Horabin, J.I., Lersch, R.A., Cline, T.W., Schedl, P. (1993). Expression fo the Sex-lethal gene is controlled at multiple levels during Drosophila oogenesis. *Development*, 118(3),797-812. PMID: 8076518.

Chang, C. H., & Larracuente, A. M. (2019). Heterochromatin-Enriched Assemblies Reveal the Sequence and Organization of the Drosophila melanogaster Y Chromosome. *Genetics*, *211*(1), 333-348. https://doi.org/10.1534/genetics.118.301765 PMC6325706

Chang, C. H., Mejia Natividad, I., & Malik, H. S. (2023). Expansion and loss of sperm nuclear basic protein genes in Drosophila correspond with genetic conflicts between sex chromosomes. *Elife*, *12*. https://doi.org/10.7554/eLife.85249 PMC9917458

Chen, X., Lu, C., Morillo Prado, J. R., Eun, S. H., & Fuller, M. T. (2011). Sequential changes at differentiation gene promoters as they become active in a stem cell lineage. *Development*, *138*(12), 2441-2450. https://doi.org/10.1242/dev.056572 PMC3100706

Di Cara, F., Morra, R., Cavaliere, D., Sorrentino, A., De Simone, A., Polito, C. L., & Digilio, A. F. (2006). Structure and expression of a novel gene family showing male germline specific expression in Drosophila melanogaster. *Insect Mol Biol*, *15*(6), 813-822. https://doi.org/10.1111/j.1365-2583.2006.00688.x

Dietzel, S., Niemann, H., Bruckner, B., & Paro, R. (1999). The nuclear distribution of Polycomb during Drosophila development shown with a GFP fusion protein. *Chromosoma*, 108(2), 83-94. PMID: 10382070.

El-Sharnouby, S., Redhouse, J., & White, R. A. (2013). Genome-wide and cell-specific epigenetic analysis challenges the role of polycomb in Drosophila spermatogenesis. *PLoS Genet*, *9*(10), e1003842. https://doi.org/10.1371/journal.pgen.1003842 PMC3798269

Ernst, C., Eling, N., Martinez-Jimenez, C. P., Marioni, J. C., & Odom, D. T. (2019). Staged developmental mapping and X chromosome transcriptional dynamics during mouse spermatogenesis. *Nat Commun*, *10*(1), 1251. https://doi.org/10.1038/s41467-019-09182-1 PMC6424977

Fingerhut, J. M., Moran, J. V., & Yamashita, Y. M. (2019). Satellite DNA-containing gigantic introns in a unique gene expression program during Drosophila spermatogenesis. *PLoS Genet*, *15*(5), e1008028. https://doi.org/10.1371/journal.pgen.1008028 PMC6508621

Freiman, R. N. (2009). Specific variants of general transcription factors regulate germ cell development in diverse organisms. *Biochim Biophys Acta*, *1789*(3), 161-166. https://doi.org/10.1016/j.bbagrm.2009.01.005 PMC2686221

Gorfinkiel, N., Fanti, L., Melgar, T., García, E., Pimpinelli, S., Guerrero, I., & Vidal, M. (2004). The Drosophila Polycomb group gene Sex combs extra encodes the ortholog of mammalian Ring1 proteins. *Mech Dev*, *121*(5), 449-462. https://doi.org/10.1016/j.mod.2004.03.019

Grossniklaus, U., & Paro, R. (2014). Transcriptional silencing by polycomb-group proteins. *Cold Spring Harb Perspect Biol*, *6*(11), a019331. https://doi.org/10.1101/cshperspect.a019331 PMC4413232

Hennig, W., & Weyrich, A. (2013). Histone modifications in the male germ line of Drosophila. *BMC Dev Biol*, *13*, 7. https://doi.org/10.1186/1471-213x-13-7 PMC3602674

Hiller, M., Chen, X., Pringle, M. J., Suchorolski, M., Sancak, Y., Viswanathan, S., Bolival, B., Lin, T. Y., Marino, S., & Fuller, M. T. (2004). Testis-specific TAF homologs collaborate to control a tissue-specific transcription program. *Development*, *131*(21), 5297-5308. https://doi.org/10.1242/dev.01314

Huynh, K. D., & Lee, J. T. (2005). X-chromosome inactivation: a hypothesis linking ontogeny and phylogeny. *Nat Rev Genet*, *6*(5), 410-418. https://doi.org/10.1038/nrg1604

Kaya-Okur, H. S., Wu, S. J., Codomo, C. A., Pledger, E. S., Bryson, T. D., Henikoff, J. G., Ahmad, K., & Henikoff, S. (2019). CUT&Tag for efficient epigenomic profiling of small samples and single cells. *Nat Commun*, *10*(1), 1930. https://doi.org/10.1038/s41467-019-09982-5 PMC6488672

Khalil, A. M., Boyar, F. Z., & Driscoll, D. J. (2004). Dynamic histone modifications mark sex chromosome inactivation and reactivation during mammalian spermatogenesis. *Proceedings of the National Academy of Sciences*, *101*(47), 16583-16587. https://doi.org/10.1073/pnas.0406325101

Laktionov, P. P., Maksimov, D. A., Romanov, S. E., Antoshina, P. A., Posukh, O. V., White-Cooper, H., Koryakov, D. E., & Belyakin, S. N. (2018). Genome-wide analysis of gene regulation mechanisms during Drosophila spermatogenesis. *Epigenetics Chromatin*, *11*(1), 14. https://doi.org/10.1186/s13072-018-0183-3 PMC5879934

Larsson, J., & Meller, V. H. (2006). Dosage compensation, the origin and the afterlife of sex chromosomes. *Chromosome Res*, *14*(4), 417-431. https://doi.org/10.1007/s10577-006-1064-3

Lawlor, M. A., Cao, W., & Ellison, C. E. (2021). A transposon expression burst accompanies the activation of Y-chromosome fertility genes during Drosophila spermatogenesis. *Nat Commun*, *12*(1), 6854. https://doi.org/10.1038/s41467-021-27136-4 PMC8617248

Li, H., Janssens, J., De Waegeneer, M., Kolluru, S. S., Davie, K., Gardeux, V., Saelens, W., David, F. P. A., Brbić, M., Spanier, K., Leskovec, J., McLaughlin, C. N., Xie, Q., Jones, R. C., Brueckner, K., Shim, J., Tattikota, S. G., Schnorrer, F., Rust, K., . . . Zinzen, R. P. (2022). Fly Cell Atlas: A single-nucleus transcriptomic atlas of the adult fruit fly. *Science*, *375*(6584), eabk2432. https://doi.org/10.1126/science.abk2432 PMC8944923

Lifschytz, E., & Lindsley, D. L. (1972). The role of X-chromosome inactivation during spermatogenesis (Drosophila-allocycly-chromosome evolution-male sterility-dosage compensation). *Proc Natl Acad Sci U S A*, *69*(1), 182-186. https://doi.org/10.1073/pnas.69.1.182 PMC427571

Lim, C., Tarayrah, L., & Chen, X. (2012). Transcriptional regulation during Drosophila spermatogenesis. *Spermatogenesis*, *2*(3), 158-166. https://doi.org/10.4161/spmg.21775 PMC3469439

Lin, T.Y., Viswanathan, S., Wood, C., Wilson, P.G., Wolf, N., Fuller, M.T. (1996). Coordinate developmental control of the meiotic cell cycle and spermatid differentiation in Drosophila males. *Development*, 122(4), 1331-1341.

Loubiere, V., Papadopoulos, G. L., Szabo, Q., Martinez, A. M., & Cavalli, G. (2020). Widespread activation of developmental gene expression characterized by PRC1-dependent chromatin looping. *Sci Adv*, *6*(2), eaax4001. https://doi.org/10.1126/sciadv.aax4001 PMC6954061

Mahadevaraju, S., Fear, J. M., Akeju, M., Galletta, B. J., Pinheiro, M., Avelino, C. C., Cabral-de-Mello, D. C., Conlon, K., Dell'Orso, S., Demere, Z., Mansuria, K., Mendonça, C. A., Palacios-Gimenez, O. M., Ross, E., Savery, M., Yu, K., Smith, H. E., Sartorelli, V., Yang, H., . . . Oliver, B. (2021). Dynamic sex chromosome expression in Drosophila male germ cells. *Nat Commun*, *12*(1), 892. https://doi.org/10.1038/s41467-021-20897-y PMC7873209

McKee, B. D., & Handel, M. A. (1993). Sex chromosomes, recombination, and chromatin conformation. *Chromosoma*, *102*(2), 71-80. https://doi.org/10.1007/bf00356023

Mu, W., Starmer, J., Fedoriw, A. M., Yee, D., & Magnuson, T. (2014). Repression of the soma-specific transcriptome by Polycomb-repressive complex 2 promotes male germ cell development. *Genes Dev*, *28*(18), 2056-2069. https://doi.org/10.1101/gad.246124.114 PMC4173155

Muniz, L., Nicolas, E., & Trouche, D. (2021). RNA polymerase II speed: a key player in controlling and adapting transcriptome composition. *Embo j*, *40*(15), e105740. https://doi.org/10.15252/embj.2020105740 PMC8327950

Parisi, M., Nutall, R., Naiman, D., Bouffard, G., Malley, J., Andrews, J., Eastman, S., & Oliver, B. (2003). Paucity of genes on the Drosophila *X* chromosome showing male-biased expression. *Science*, 299(5607), 697-700. PMID: 12511656.

Rastelli, L., & Kuroda, M. I. (1998). An analysis of maleless and histone H4 acetylation in Drosophila melanogaster spermatogenesis. *Mech Dev*, *71*(1-2), 107-117. https://doi.org/10.1016/s0925-4773(98)00009-4

Rathke, C., Baarends, W. M., Jayaramaiah-Raja, S., Bartkuhn, M., Renkawitz, R., & Renkawitz-Pohl, R. (2007). Transition from a nucleosome-based to a protamine-based chromatin configuration during spermiogenesis in Drosophila. *J Cell Sci*, *120*(Pt 9), 1689-1700. https://doi.org/10.1242/jcs.004663

Raz, A. A., Vida, G. S., Stern, S. R., Mahadevaraju, S., Fingerhut, J. M., Viveiros, J. M., Pal, S., Grey, J. R., Grace, M. R., Berry, C. W., Li, H., Janssens, J., Saelens, W., Shao, Z., Hu, C., Yamashita, Y. M., Przytycka, T., Oliver, B., Brill, J. A., . . . Fuller, M. T. (2023). Emergent dynamics of adult stem cell lineages from single nucleus and single cell RNA-Seq of Drosophila testes. *Elife*, *12*. https://doi.org/10.7554/eLife.82201 PMC9934865

Shi, Z., Lim, C., Tran, V., Cui, K., Zhao, K., & Chen, X. (2020). Single-cyst transcriptome analysis of Drosophila male germline stem cell lineage. *Development*, *147*(8). https://doi.org/10.1242/dev.184259 PMC7174844

Solari, A. J. (1974). The behavior of the XY pair in mammals. *Int Rev Cytol*, *38*(0), 273-317. https://doi.org/10.1016/s0074-7696(08)60928-6
Tasaki, T., Mulder, L. C., Iwamatsu, A., Lee, M. J., Davydov, I. V., Varshavsky, A., Muesing, M., & Kwon, Y. T. (2005). A family of mammalian E3 ubiquitin ligases that contain the UBR box motif and recognize N-degrons. *Mol Cell Biol*, *25*(16), 7120-7136. https://doi.org/10.1128/mcb.25.16.7120-7136.2005 PMC1190250
Turner, J. M. (2007). Meiotic sex chromosome inactivation. *Development*, *134*(10), 1823-1831. https://doi.org/10.1242/dev.000018
Turner, J. M. (2015). Meiotic Silencing in Mammals. *Annu Rev Genet*, *49*, 395-412. https://doi.org/10.1146/annurev-genet-112414-055145
Vibranovski, M. D. (2014). Meiotic sex chromosome inactivation in Drosophila. *J Genomics*, *2*, 104-117. https://doi.org/10.7150/jgen.8178 PMC4105432
Wang, H., Wang, L., Erdjument-Bromage, H., Vidal, M., Tempst, P., Jones, R. S., & Zhang, Y. (2004). Role of histone H2A ubiquitination in Polycomb silencing. *Nature*, *431*(7010), 873-878. https://doi.org/10.1038/nature02985
White-Cooper, H., & Bausek, N. (2010). Evolution and spermatogenesis. *Philos Trans R Soc Lond B Biol Sci*, *365*(1546), 1465-1480. https://doi.org/10.1098/rstb.2009.0323 PMC2871925
White-Cooper, H., D'Alessio, J. A., Wright, K. J., & Tjian, R. (2010). Molecular mechanisms of gene regulation during Drosophila spermatogenesis
Shifting players and paradigms in cell-specific transcription. *Reproduction*, *139*(1), 11-21. https://doi.org/10.1186/gb-2010-11-4-r42
10.1530/rep-09-0083 2884545
Witt, E., Benjamin, S., Svetec, N., & Zhao, L. (2019). Testis single-cell RNA-seq reveals the dynamics of de novo gene transcription and germline mutational bias in Drosophila. *Elife*, *8*. https://doi.org/10.7554/eLife.47138 PMC6697446
Witt, E., Shao, Z., Hu, C., Krause, H. M., & Zhao, L. (2021). Single-cell RNA-sequencing reveals pre-meiotic X-chromosome dosage compensation in Drosophila testis. *PLoS Genet*, *17*(8), e1009728. https://doi.org/10.1371/journal.pgen.1009728 PMC8396764

Supplementary Information

Supplementary Tables

Supplementary Table 1. Sample IDs and sequencing results.

Supplementary Table 2. snRNA-seq gene expression scores and H3K4me2 enrichment at Drosophila promoters. This lists unique TSSs in the Flybase dm6 r6.31 assembly release and associated gene expression scores (derived from Raz 2023) and H3K4me2 signal (in CPM) in a -200–+500 bp window around each TSS.

Supplementary Table 3. Enrichment of RNAPIIS2p, H3K9me2, H3K27me3, and uH2A across Drosophila genes in dissociated testes, in isolated spermatocytes, and in wing imaginal discs. This lists unique genes in the Flybase dm6 r6.31 assembly release and associated gene expression scores (derived from Raz 2023) and chromatin profiling signals (in CPKM) across each gene length.

Supplementary Table 4. Enrichment of RNAPIIS2p, H3K9me2, H3K27me3, and uH2A across consensus transposon sequences in dissociated testes, in isolated spermatocytes, and in wing imaginal discs. This lists a subset of transposon consensus sequences

907 (https://github.com/bergmanlab/drosophila-
908 transposons/blob/master/misc/D_mel_transposon_sequence_set.fa) and associated chromatin
909 profiling signals (in CPKM) across each consensus length.

910

911 **Supplementary Figures**

912 **Supplementary Figure 1. Genes with germline-enriched expression in testes.**
913 (**A**) FCA clustering. Number of promoters in each cluster is marked on the left.
914 (**B**) MA plot and threshold for germline-enriched genes (snRNA-seq data showing gexp/sexp with
915 ≥1 cut-off). Red marks genes in germline-expressed clusters 1-5, and blue marks genes in testes
916 somatic clusters 6-10. The threshold for assigning genes with germline-enriched expression is in
917 green.
918

919 **Supplementary Figure 2. Distribution of elongating RNAPII in spermatocytes and in somatic**
920 **cells.** Heatmap of RNAPIIS2p signal around gene TSSs in spermatocytes, in dissociated testes,
921 and in wing imaginal discs.
922

923 **Supplementary Figure 3. Chromatin features across transposon consensus sequences in**
924 **spermatocytes and in somatic cells.**
925 Selected transposons with increased RNAPIIS2p signal in spermatocytes *versus* wing imaginal
926 discs (log2FC≥2).
927

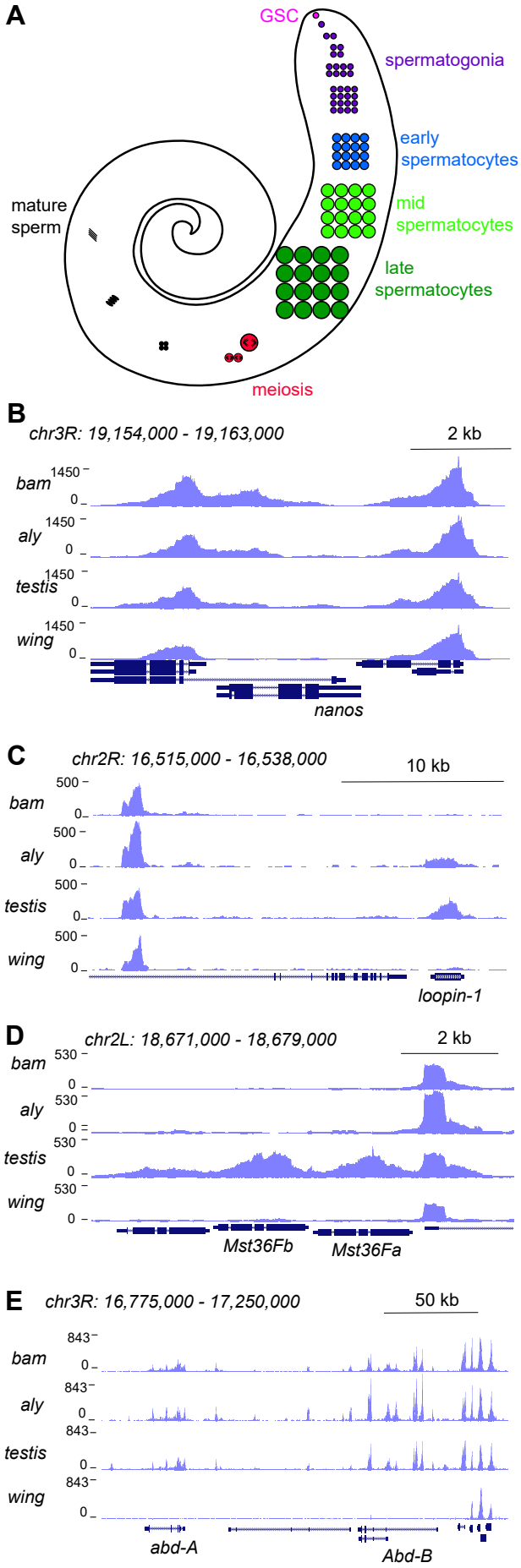
A
GSC
spermatogonia
early
spermatocytes
mid
spermatocytes
late
spermatocytes
mature
sperm
meiosis
B
chr3R: 19,154,000 - 19,163,000
2 kb
bam
aly
testis
wing
1450
0
nanos
C
chr2R: 16,515,000 - 16,538,000
10 kb
bam
aly
testis
wing
500
0
loopin-1
D
chr2L: 18,671,000 - 18,679,000
2 kb
bam
aly
testis
wing
530
0
Mst36Fb
Mst36Fa
E
chr3R: 16,775,000 - 17,250,000
50 kb
bam
aly
testis
wing
843
0
abd-A
Abd-B

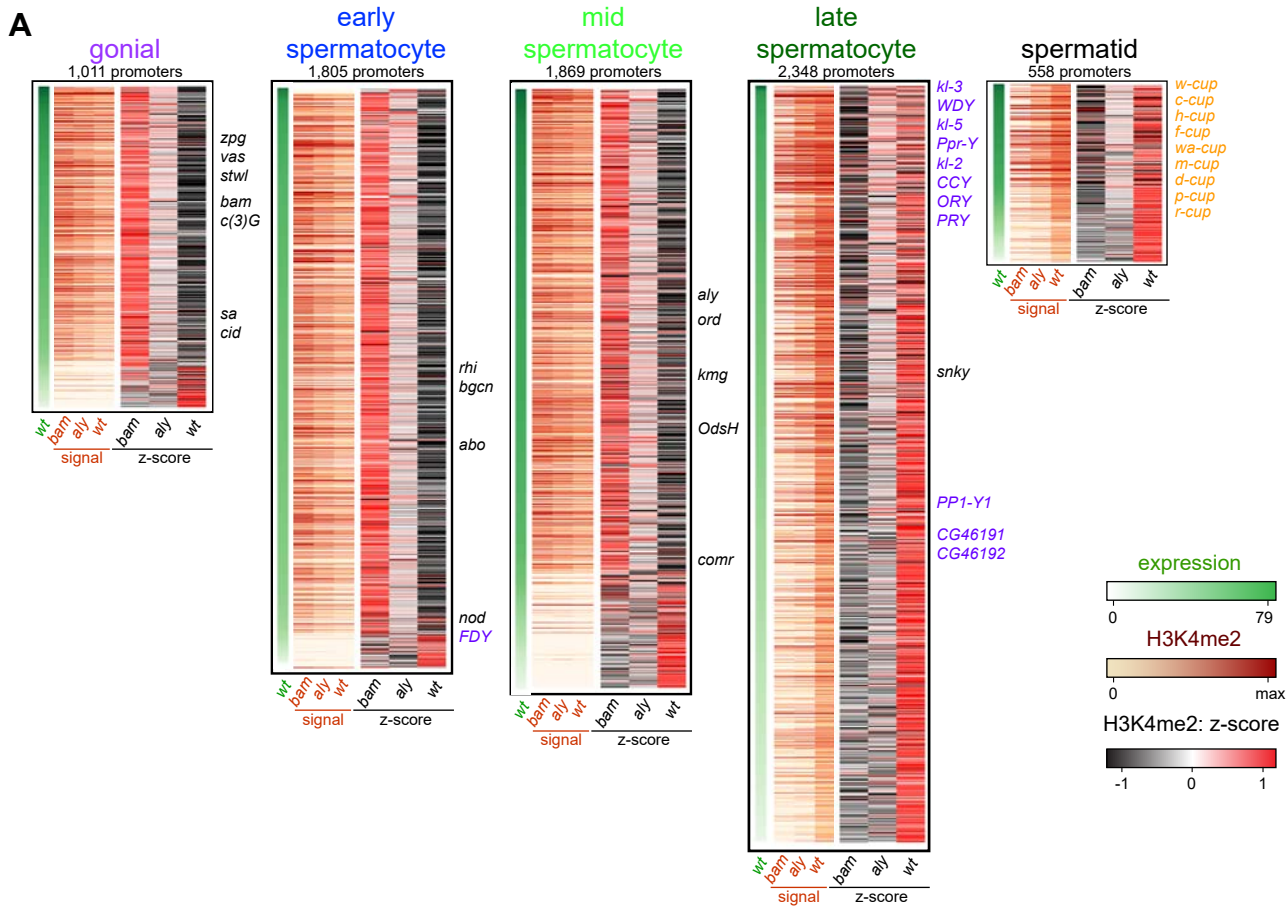
A
gonial
1,011 promoters
early spermatocyte
1,805 promoters
mid spermatocyte
1,869 promoters
late spermatocyte
2,348 promoters
spermatid
558 promoters
zpg
vas
stwl
bam
c(3)G
sa
cid
rhi
bgcn
abo
nod
FDY
aly
ord
kmg
OdsH
comr
kl-3
WDY
kl-5
Ppr-Y
kl-2
CCY
ORY
PRY
snky
PP1-Y1
CG46191
CG46192
w-cup
c-cup
h-cup
f-cup
wa-cup
m-cup
d-cup
p-cup
r-cup
wt
bam
aly
wt
signal
z-score
expression
0
79
H3K4me2
0
max
H3K4me2: z-score
-1
0
1

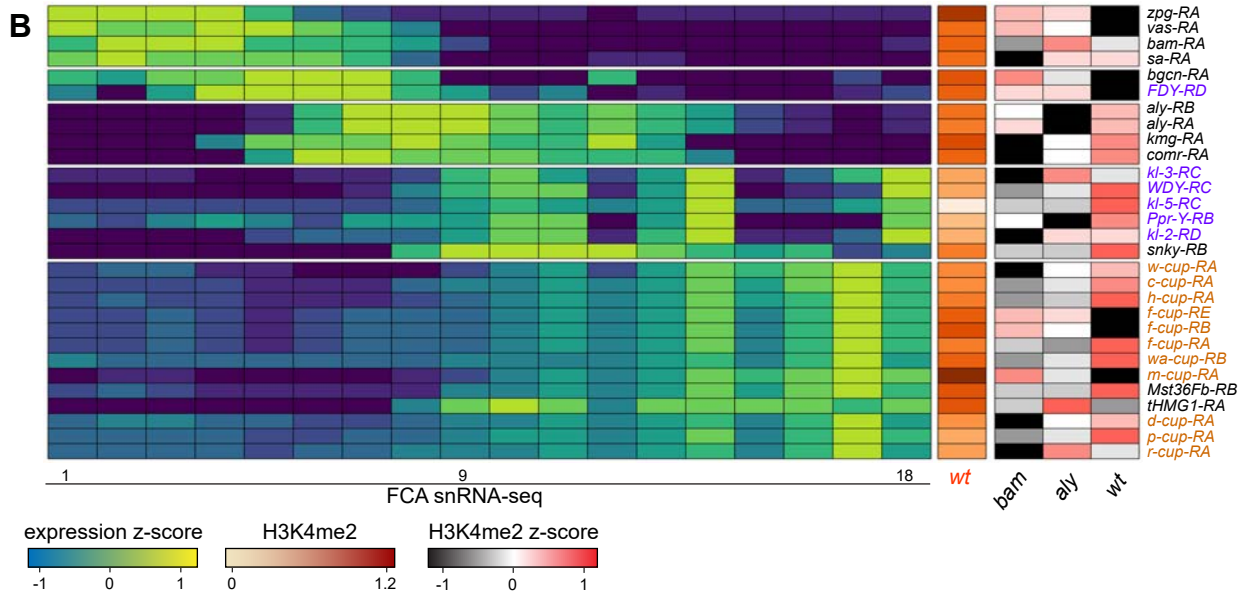
B
zpg-RA
vas-RA
bam-RA
sa-RA
bgcn-RA
FDY-RD
aly-RB
aly-RA
kmg-RA
comr-RA
kl-3-RC
WDY-RC
kl-5-RC
Ppr-Y-RB
kl-2-RD
snky-RB
w-cup-RA
c-cup-RA
h-cup-RA
f-cup-RE
f-cup-RB
f-cup-RA
wa-cup-RB
m-cup-RA
Mst36Fb-RB
tHMG1-RA
d-cup-RA
p-cup-RA
r-cup-RA
1
9
18
FCA snRNA-seq
wt
bam
aly
wt
expression z-score
-1
0
1
H3K4me2
0
1.2
H3K4me2 z-score
-1
0
1

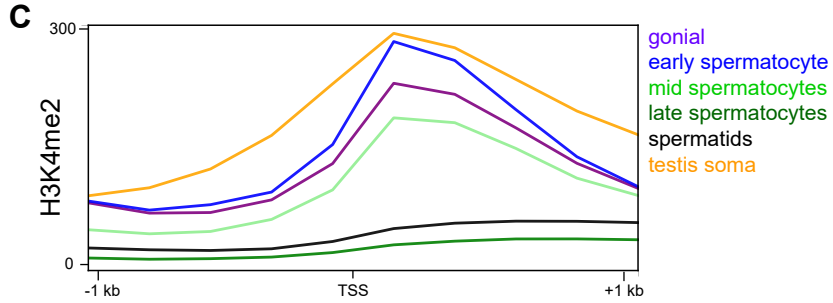
C
300
0
H3K4me2
-1 kb
TSS
+1 kb
gonial
early spermatocyte
mid spermatocytes
late spermatocytes
spermatids
testis soma

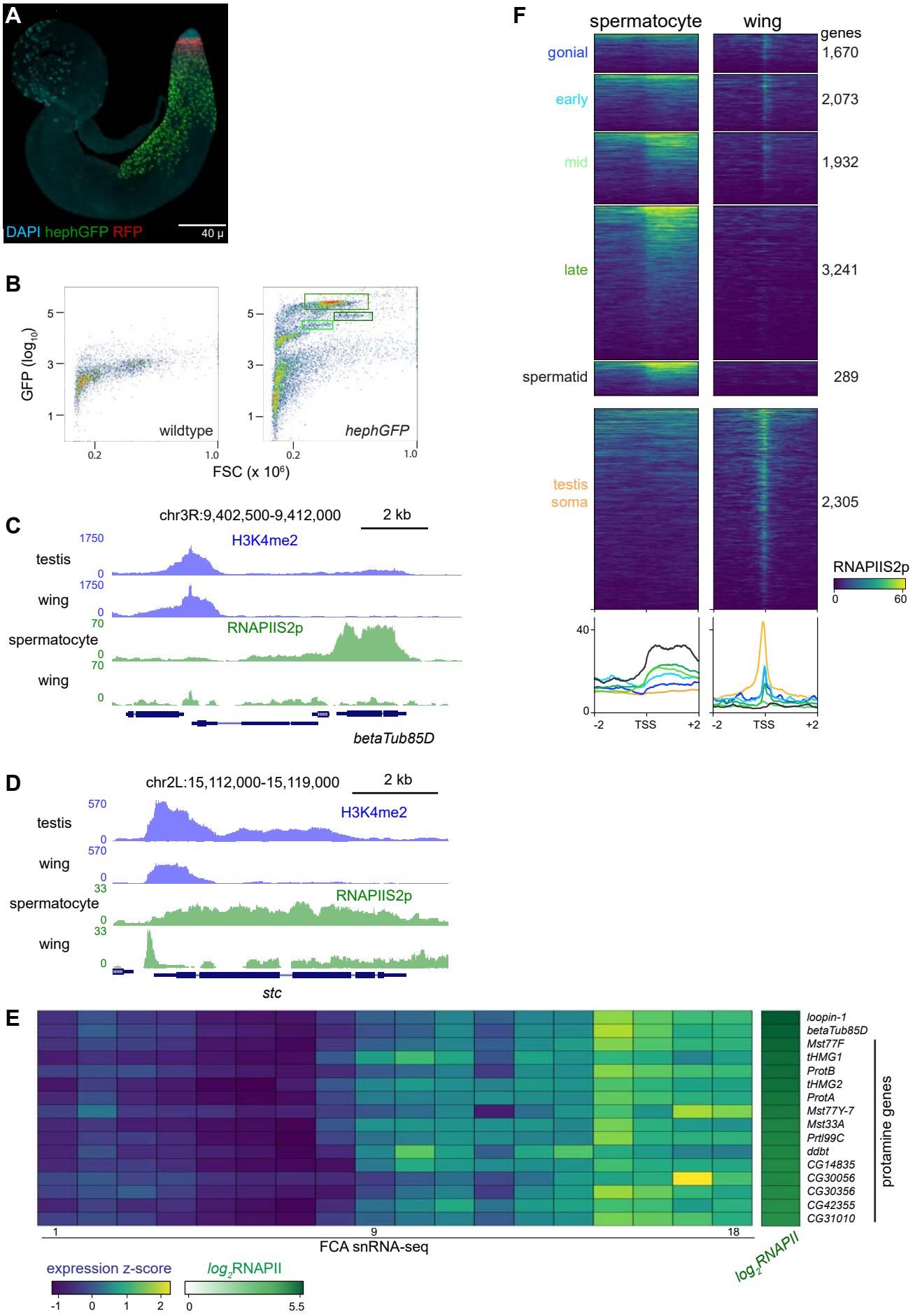
A
DAPI hephGFP RFP
40 µ
B
GFP (log10)
wildtype
hephGFP
FSC (x 10^6)
C
chr3R:9,402,500-9,412,000
2 kb
H3K4me2
testis
wing
RNAPIIS2p
spermatocyte
betaTub85D
D
chr2L:15,112,000-15,119,000
stc
E
FCA snRNA-seq
expression z-score
log2RNAPII
protamine genes
loopin-1
betaTub85D
Mst77F
tHMG1
ProtB
tHMG2
ProtA
Mst77Y-7
Mst33A
Prtl99C
ddbt
CG14835
CG30056
CG30356
CG42355
CG31010
F
spermatocyte
wing
genes
gonial
1,670
early
2,073
mid
1,932
late
3,241
spermatid
289
testis soma
2,305
RNAPIIS2p
TSS

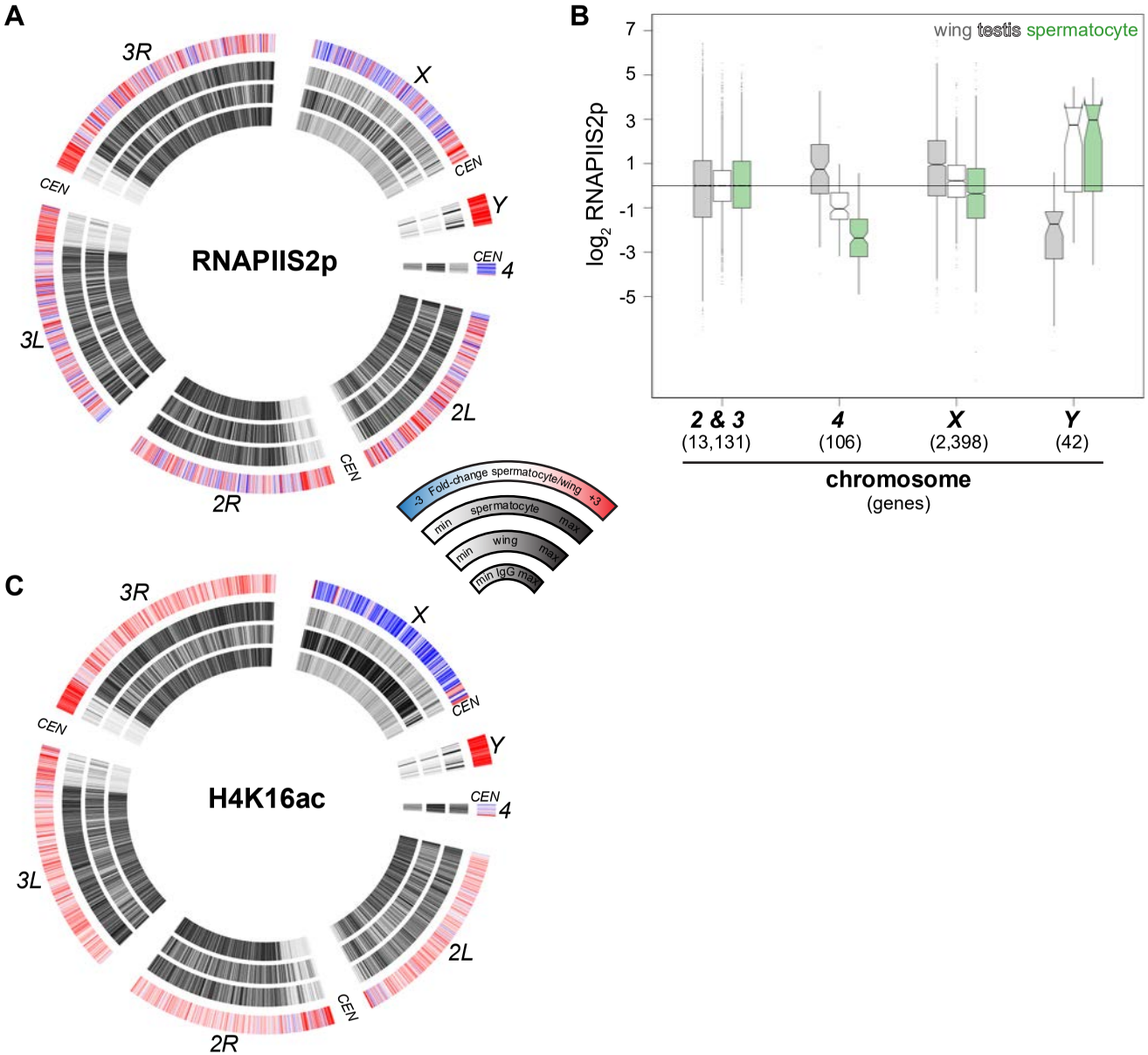
A
3R
X
CEN
CEN
Y
RNAPIIS2p
CEN
4
3L
2L
CEN
2R
-3 Fold-change spermatocyte/wing +3
min spermatocyte max
min wing max
min IgG max
B
wing testis spermatocyte
log2 RNAPIIS2p
7
5
3
1
-1
-3
-5
2 & 3
(13,131)
4
(106)
X
(2,398)
Y
(42)
chromosome
(genes)
C
3R
X
CEN
CEN
Y
H4K16ac
CEN
4
3L
2L
CEN
2R

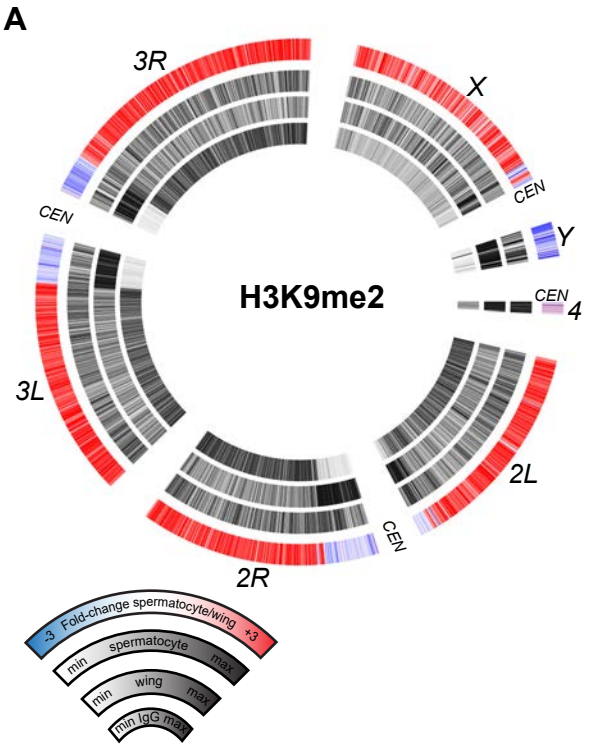
A
3R
X
CEN
CEN
Y
H3K9me2
CEN
4
3L
2L
CEN
2R
-3
Fold-change spermatocyte/wing
+3
min
spermatocyte
max
min
wing
max
min IgG max

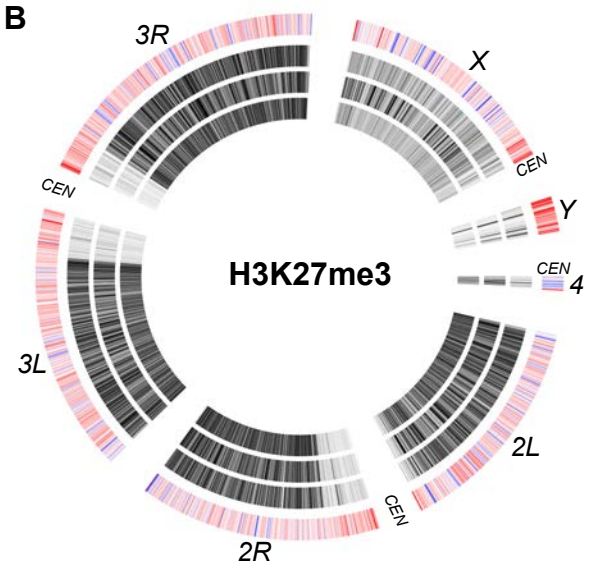
B
3R
X
CEN
CEN
Y
H3K27me3
CEN
4
3L
2L
CEN
2R

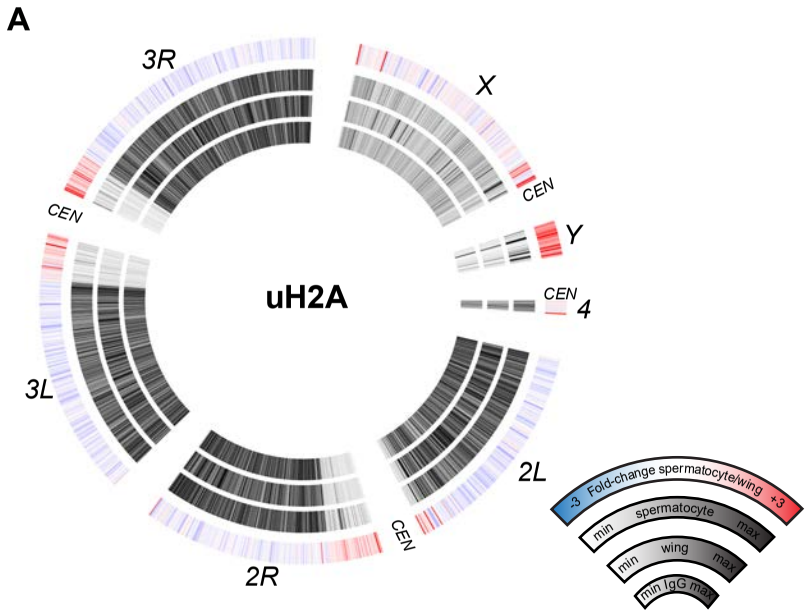
A
3R
X
CEN
CEN
Y
uH2A
CEN
4
3L
2L
CEN
2R
-3 Fold-change spermatocyte/wing +3
min spermatocyte max
min wing max
min IgG max

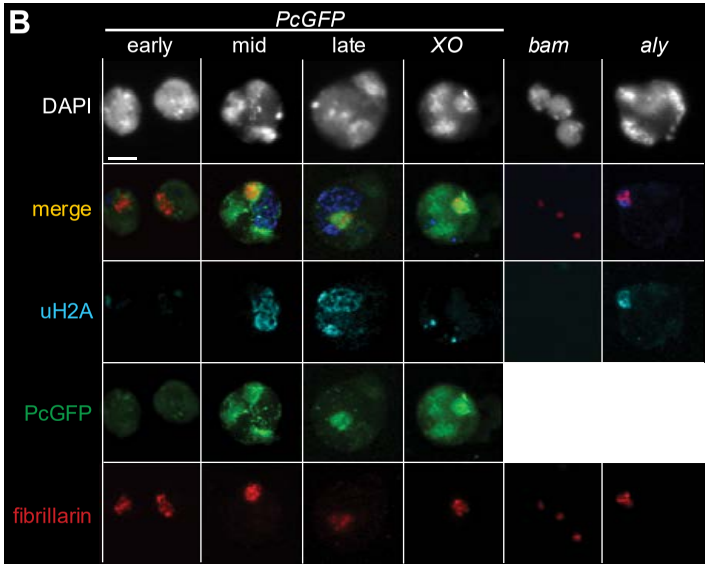
B
PcGFP
early
mid
late
XO
bam
aly
DAPI
merge
uH2A
PcGFP
fibrillarin

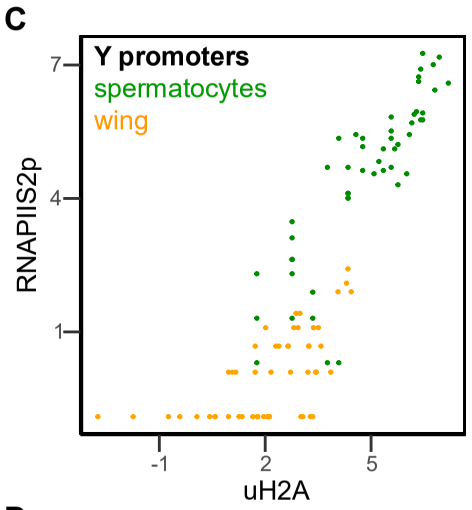
C
Y promoters
spermatocytes
wing
RNAPIIS2p
7
4
1
-1
2
5
uH2A

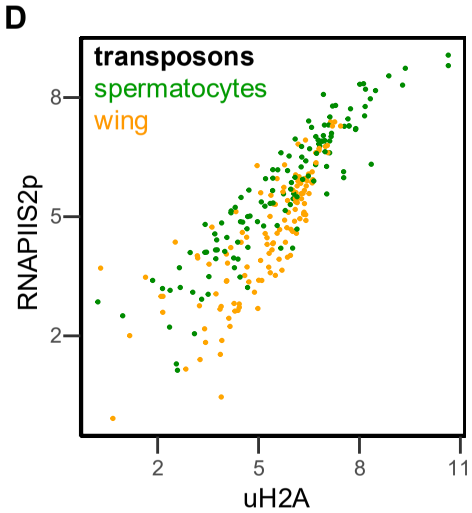
D
transposons
spermatocytes
wing
RNAPIIS2p
8
5
2
2
5
8
11
uH2A